Structural, Kinetic, and Mutational Studies of the Zinc Ion Environment in Tetrameric Cytidine Deaminase[†,‡]

Eva Johansson,*[,§,||] Jan Neuhard,[⊥] Martin Willemoës,[§] and Sine Larsen[§,||]

Centre for Crystallographic Studies, Department of Chemistry, University of Copenhagen, Universitetsparken 5, DK-2100 Copenhagen Ø, Denmark, European Synchrotron Radiation Facility, BP 220, F-38043 Grenoble Cedex, France, and Institute of Molecular Biology, University of Copenhagen, Sølvgade 83H, DK-1307 Copenhagen K, Denmark

Received October 22, 2003; Revised Manuscript Received February 27, 2004

ABSTRACT: The zinc-containing cytidine deaminase (CDA, EC 3.5.4.5) is a pyrimidine salvage enzyme catalyzing the hydrolytic deamination of cytidine and 2′-deoxycytidine forming uridine and 2′-deoxyuridine, respectively. Homodimeric CDA (D-CDA) and homotetrameric CDA (T-CDA) both contain one zinc ion per subunit coordinated to the catalytic water molecule. The zinc ligands in D-CDA are one histidine and two cysteine residues, whereas in T-CDA zinc is coordinated to three cysteines. Two of the zinc coordinating cysteines in T-CDA form hydrogen bonds to the conserved residue Arg56, and this residue together with the dipole moments from two α-helices partially neutralizes the additional negative charge in the active site, leading to a catalytic activity similar to D-CDA. Arg56 has been substituted by a glutamine (R56Q), the corresponding residue in D-CDA, an alanine (R56A), and an aspartate (R56D). Moreover, one of the zinc-liganding cysteines has been substituted by histidine to mimic D-CDA, alone (C53H) and in combination with R56Q (C53H/R56Q). R56A, R56Q, and C53H/R56Q contain the same amount of zinc as the wild-type enzyme. The zinc-binding capacity of R56D is reduced. Only R56A, R56Q, and C53H/R56Q yielded measurable CDA activity, R56A and R56Q with similar K_m but decreased V_{max} values compared to wild-type enzyme. Because of dissociation into its inactive subunits, it was impossible to determine the kinetic parameters for C53H/R56Q. R56A and C53H/R56Q display increased apparent pK_a values compared to the wild-type enzyme and R56Q. On the basis of the structures of R56A, R56Q, and C53H/R56Q an explanation is provided of kinetic results and the apparent instability of C53H/R56Q.

Cytidine deaminase (CDA, EC 3.5.4.5)[1] catalyzes the pyrimidine salvage reaction whereby cytidine and 2′-deoxycytidine is deaminated to uridine and 2′-deoxyuridine, respectively (*1*). CDA is a zinc-containing enzyme, and the metal ion is essential for catalysis. Two classes of CDA have been found in nature: a homodimeric class (D-CDA) with a subunit molecular mass of about 32 kDa, and a homotetrameric class (T-CDA) with a molecular mass of approximately 15 kDa. D-CDAs are found in Gram-negative bacteria such as *Escherichia coli* and in plants, whereas T-CDAs are found in Gram-positive bacteria such as *Bacillus subtilis* and in many eukaryotes including mammals (*2*). The crystal structures of T-CDA from *B. subtilis* (*2*) and D-CDA from *E. coli* (*3*) have been determined. Both classes of CDAs contain one firmly bound, catalytic zinc ion per subunit. The subunit of the *E. coli* enzyme contains two domains with the same fold as that of the T-CDA subunit, resulting in similar structural cores of D-CDA and T-CDA (Figure 1). However, since only one of the D-CDA domains in each subunit binds zinc, there are only two active sites per enzyme molecule in contrast to four in the T-CDA. The active sites in T-CDA are made from residues from three of the four subunits of the tetramer (Figure 1a). In D-CDA, each active site is formed by residues from both subunits. T-CDAs differ also from D-CDAs in having three cysteine residues as ligands for the catalytic zinc ion, while in D-CDA one of the cysteine residues is replaced by a histidine residue. Zinc ions coordinated by three cysteine residues have been observed to play a role for structural stability (*4*), but are rarely associated with catalytic activity. A CDA-related enzyme, Blasticidin S deaminase, that catalyzes the deamination of the antibiotic Blasticidin S is a homotetrameric zinc enzyme that also has three cysteine residues as zinc ion ligands (*5*, *6*). The metal specificity of *B. subtilis* T-CDA has previously been examined, showing that addition of Cd^{2+}

[†] This work was supported by grants from the Hellmuth Hertz Foundation and the Danish National Research Foundation.

[‡] The atomic coordinates and observed structure factor amplitudes have been deposited in the Protein Data Bank under accession codes 1UWZ, 1UX0, and 1UX1 for R56A, R56Q, and C53H/R56Q, respectively.

* To whom correspondence should be addressed: Phone: (+45) 35 32 02 79 Fax: (+45) 35 32 02 99. E-mail: eva@ccs.ki.ku.dk.

[§] Centre for Crystallographic Studies, University of Copenhagen.

[||] European Synchrotron Radiation Facility.

[⊥] Institute of Molecular Biology, University of Copenhagen.

[1] Abbreviations: CDA, cytidine deaminase (EC 3.5.4.5); C53H, *B. subtilis* T-CDA with a Cys53-to-His substitution; C53H/R56Q, *B. subtilis* T-CDA with a Cys53-to-His and an Arg56-to-Glu substitution; D-CDA, dimeric cytidine deaminase; DTT, dithiotreitol; IPTG, isopropyl-1-thio-β-D-galactopyranosid; MPD, 2-methyl-2,4-pentanediol; NCS, noncrystallographic symmetry; R56A, *B. subtilis* T-CDA with an Arg56-to-Ala substitution; R56D, *B. subtilis* T-CDA with an Arg56-to-Asp substitution; R56Q, *B. subtilis* T-CDA with an Arg56-to-Glu substitution; rmsd, root-mean-square deviation; SDS−PAGE, sodium dodecyl sulfate−polyacrylamide gel electrophoresis; T-CDA, tetrameric cytidine deaminase; THU, 3,4,5,6-tetrahydro-2′-deoxyuridine.

10.1021/bi035893x CCC: $27.50
Published on Web 04/30/2004

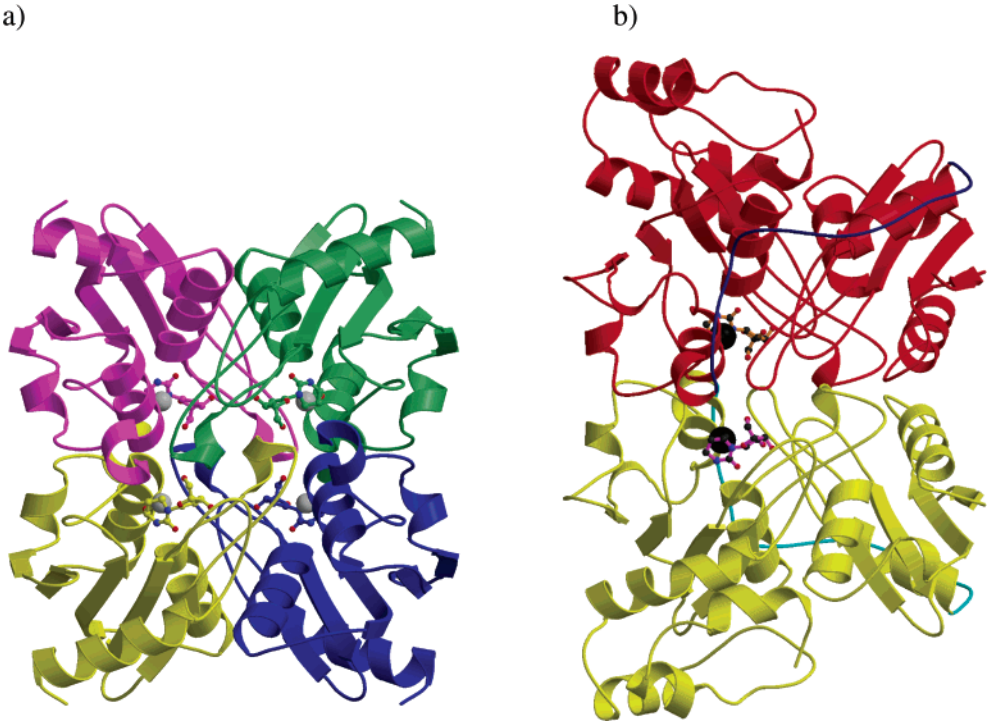

FIGURE 1: Cartoons of (a) T-CDA from *B. subtilis* and (b) D-CDA from *E. coli*. The subunits of T-CDA are shown in purple, green, yellow, and blue, respectively. The subunits of D-CDA are shown in red and yellow with the respective linkers between the catalytic and the C-terminal domain in blue and cyan. The zinc ions and the bound inhibitors are shown in ball-and-stick representations. The pictures were prepared with MOLSCRIPT (*38*) and Raster3D (*39*).

or Co^{2+} to the apo enzyme cause partial reactivation, whereas other divalent metal ions, such as Fe^{2+}, Ni^{2+}, Mn^{2+}, Mg^{2+}, and Cu^{2+} failed to promote reactivation (*7*).

Other enzymes catalyzing deamination of a cytosine ring are cytosine, dCMP, and dCTP deaminases, respectively. As expected from sequence comparisons, the crystal structures of bacterial and yeast cytosine deaminases revealed completely different folds. The *E. coli* enzyme is hexameric with $(\alpha\beta)_8$ barrel subunits (*8*), and the yeast enzyme is homodimeric with a subunit fold similar to T-CDA (*9*, *10*). The active sites show some similarity and contain an iron ion and a zinc ion for the bacterial and the yeast enzymes, respectively. The metal liganding residues in these enzymes are four histidine residues and one aspartate for the iron ion in *E. coli* cytosine deaminase, and one histidine and two cysteine residues for the zinc ion in the yeast enzyme, which is very similar to the zinc coordination in D-CDA. The bacterial and yeast cytosine deaminases is an example of convergent evolution, which is underlined by the fact that their reaction intermediates have opposite chiralities. dCMP deaminases are also zinc-containing enzymes (*11*), but the three-dimensional structure of this enzyme is not known. dCTP deaminating enzymes, on the other hand, are working with totally different catalytic machinery, which does not involve a catalytic metal ion. This has been shown for the *E. coli* dCTP deaminase (*12*) and for the bifunctional dCTP deaminase-dUTPase from the hyperthermophilic archaeon *Methanocaldococcus jannaschii* (*13*−*16*).

Zinc is the most common metal ion used for activation of nucleophilic hydroxide ions in metalloenzymes catalyzing hydrolysis or hydration reactions (*17*). The role of the zinc ion in CDA is to deprotonate a water molecule creating a nucleophilic hydroxyl ion that can react with the substrate. The zinc ion and its coordinating amino acid residues influence the pK_a values of the coordinated solvent. Furthermore, it is known that amino acid residues that form hydrogen bonds with metal ligands exert an electrostatic effect on the metal ion and its chemistry, like it was demonstrated for carbonic anhydrase (*18*). The two forms of CDA display similar catalytic activity despite the three negatively charged zinc ligands in T-CDA. A possible explanation for this was derived from the crystal structure of *B. subtilis* T-CDA (*2*). An arginine residue (Arg56), which forms hydrogen bonds to two of the cysteine residues (Cys 53 and Cys89; Figure 2a), and the positive end of the dipoles of two α-helices hosting these cysteine residues, contribute to neutralizing the negative charge caused by the three cysteine ligands. In the present study, the charge neutralizing residue Arg56 has been substituted by an alanine residue (R56A), an aspartate residue (R56D), and a glutamine residue (R56Q). The alanine substitution was chosen to examine enzymatic activity with an uncharged residue that cannot hydrogen bond to the cysteine residues coordinating the zinc ion. This mutant enzyme would also help in understanding the importance of the charge from the helix dipoles only. Substitution of the positively charged arginine residue by an aspartate residue was performed with the intention of studying the effect of introducing additional negative charge. Finally, glutamine is the residue corresponding to Arg56 in D-CDA. It possesses the hydrogen bonding capacity but not the charge of Arg56. To mimic the zinc coordination in D-CDA, the zinc-coordinating residue Cys53 was substituted by a histidine residue (C53H), its counterpart in D-CDA. The effect of the C53H mutation was studied both alone and in combination with the R56Q mutation, thereby creating

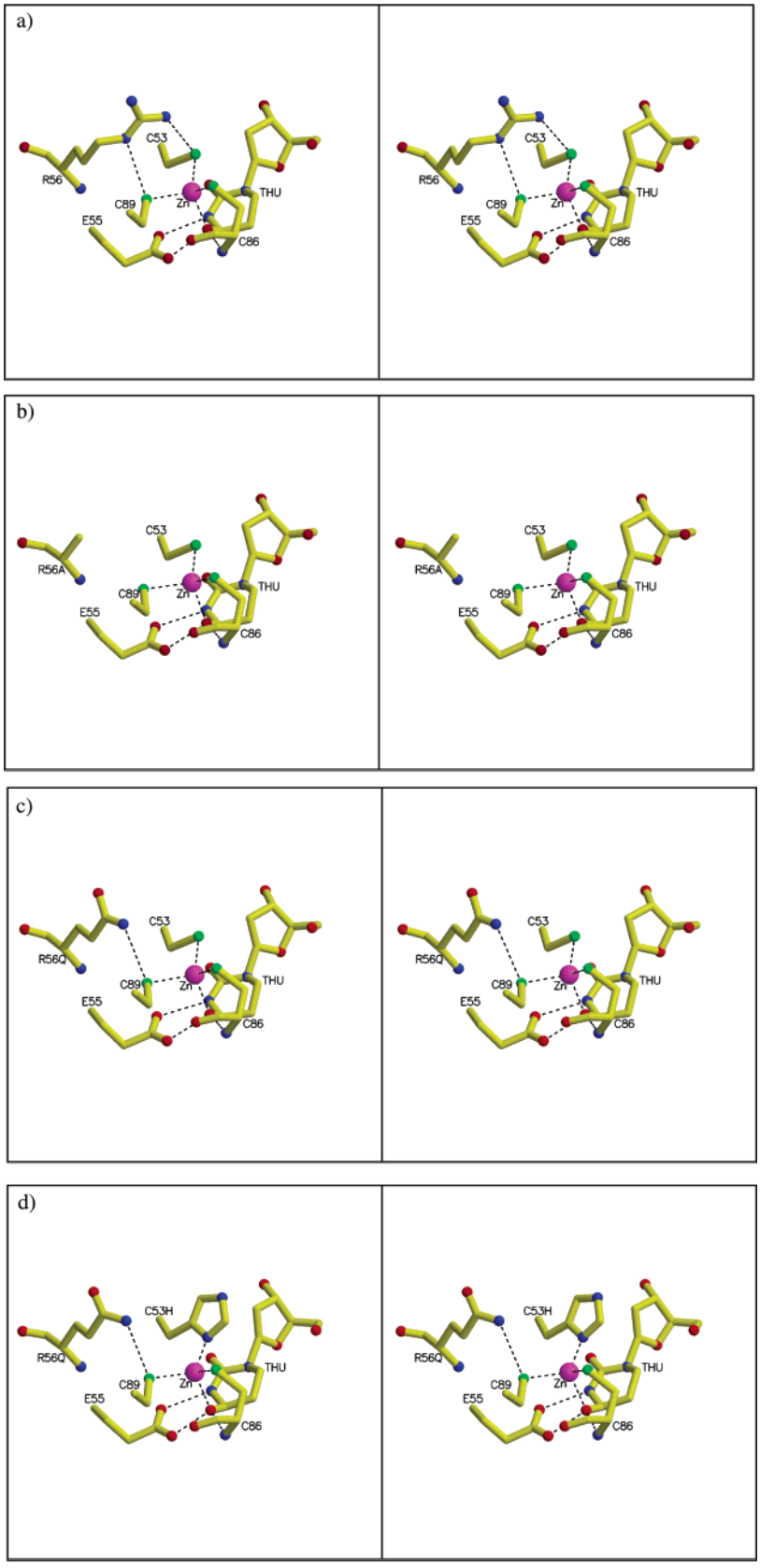

FIGURE 2: Stereoview of the active site of (a) wild-type *B. subtilis* T-CDA, (b) R56A, (c) R56Q, and (d) C53H/R56Q. Hydrogen bonds and metal ligand interactions are displayed as broken lines. The pictures were prepared with MOLSCRIPT (*38*) and Raster3D (*39*).

an active site environment similar to that found in D-CDA. Structural and kinetic studies of the T-CDA mutant enzymes presented here have provided new detailed information on the zinc-catalyzed cytidine deaminase reaction.

MATERIALS AND METHODS

Materials. Ampicillin, kanamycin, streptomycin sulfate, cytidine, deoxycytidine, Tris, HEPES, dithiothreitol (DTT),

2-methyl-2,4-pentanediol (MPD), and isopropyl-1-thio-β-D-galactopyranosid (IPTG) were obtained from Sigma-Aldridge (St. Louis, MO). 3,4,5,6-Tetrahydro-2′-deoxyuridine (THU) was purchased from Calbiochem (La Jolla, CA). The restriction endonucleases and Vent DNA polymerase were purchased by New England BioLabs, Inc., MA. The primers were obtained from MWG AG Biotech (Germany).

Bacterial Strains and Growth Conditions. The cytidine deaminase negative, pyrimidine requiring strain *E. coli* SØ5201 (MC1061*cdd::Tn10 pyrD::Kan*) was employed as host for all clonings as well as for overexpression of certain mutant CDAs. *E. coli* JF611 (*cdd pyrE argE his proA thr leu thi*), obtained from Jim Friesen, was used for overexpression of wild-type *B. subtilis* T-CDA, R56Q, and R56A. Strains were grown at 37 °C in AB minimal medium (*19)* containing 0.2% glucose and 0.2% vitamin-free casamino acids. When required, the medium was supplied with uracil (20 μg/mL), thiamine (0.5 μg/mL), ampicillin (100 μg/mL), and kanamycin (30 μg/mL). As a rich medium NZY broth (modified LB medium; *20*) was used. Solid media were prepared by adding 1.5% agar to the respective liquid media.

DNA Techniques. E. coli was made competent by treatment with $CaCl_2$ (*21*). Plasmids were isolated from *E. coli* by the alkaline/SDS lysis procedure (*22*). Endonuclease digestion and ligation of DNA was done according to the suppliers' recommendations. DNA sequencing was performed by the chain termination method (*23*) using the BigDye Terminator Cycle Sequencing kit (PE Applied Biosystems, Warrington, Great Britain) and an ABI PRISM 310 Genetic analyzer (PE Applied Biosystems, Warrington, Great Britain).

Plasmids and Site-Directed Mutagenesis. The expression vector pTrc99-A (Pharmacia) was used for all clonings. The wild-type *B. subtilis* CDA was obtained as a PCR fragment using the primers 5′wtCDA (5′GGAATGTACTCATGAACAGACAAG) and 3′wtCDA (5′CGCGGATCCT*TTA*AAGCTTTCGTTCGTCATGTAAATC) which cover the start and stop codons of CDA, respectively, shown in italics. To facilitate subsequent cloning, a *Bsp*HI site (TCATGA, underlined) overlapping the start codon and a *Bam*HI site (GGATCC, underlined) following the stop codon was introduced with the primers. pSO143 (*24*) was used as template. Following digestion with *Bsp*HI and *Bam*HI the 464-bp fragment was inserted into *Nco*I/*Bam*HI digested pTrc99-A, yielding pTrcwtCDA. Plasmids pTrcR56ACDA and pTrcR56QCDA were constructed in three steps using the megaprimer method (*25*). Pairs of complementary primers harboring the desired mutations (5′R56A: 5′CAATTGCGCCGAGgcTACCGCTTTATTTAAAGCTGTTTC; 3′R56A: 5′GCTTTAAATAAAGCGGTAgcCTCGGCGCAA; 5′R56Q: 5′CAATTGCGCCGAGCagACCGCTTTATTTAAAGCTGTTTC; 3′R56Q: 5′GCTTTAAATAAAGCGGTctGCTCGGCGCAA, mutations indicated by lower case letters) was employed in separate PCR reactions together with the 5′wtCDA and 3′wtCDA primers, respectively, using pSO143 as template. The two megaprimers produced in these reactions were used in a third PCR amplification in the presence of 5′wtCDA and 3′wtCDA. The resulting amplicon was digested with *Bsp*HI and *Bam*HI and cloned into pTrc99-A as above. The plasmids containing the R56D, C53H, and C53H/R56D mutations, i.e., pTrcR56DCDA, pTrcC53HCDA, and pTrcC53H/R56QCDA were each constructed using a single PCR amplification according to the QuickChange protocol (Stratagene, La Jolla, CA). For each mutant gene, a pair of complementary primers was used, each containing the desired mutation in the center of the primer (5′R56D: 5′GCAATTGCGCCGAGgaTACCGCTTTATTTAAAGC; 3′R56D: 5′GCTTTAAATAAAGCGGTAtcCTCGGCGCAATTGC; 5′C53H: 5′ GCATACAGCATGTGCAATcaCGCCGAGCGTACCG; 3′C53H: 5′ CGGTACGCTCGGCGtgATTGCACATGCTGTATGC; 5′C53H/R56Q: 5′ GCATACAGCATGTGCAATcaCGCCGAGCagACCG; 3′C53H/R56Q: 5′ CGGTctGCTCGGCGtgATTGCACATGCTGTATGC, mutations indicated by lower case letters). As template pTrcwtCDA (for R56D and C53H) or pTrcR56Q (for C53H/R56Q) was used. Following digestion with *Dpn*I, to degrade the template strands, the entire reaction mixture was used to transform *E. coli* SØ5201 to ampicillin resistance. In all PCR amplification reactions, Vent DNA polymerase was employed. The primary structures of all inserts were verified by DNA sequencing.

Expression and Purification of Recombinant Enzymes. Cultures (500 mL) of *E. coli* JF611 harboring pTrcwtCDA, pTrcR56QCDA, and pTrcR56ACDA and *E. coli* SØ5201 harboring pTrcR56DCDA and pTrcC53H/R56QCDA were grown exponentially at 37 °C in NZY with ampicillin. At a cell density of 10^8 cells per milliliter, 0.3 mM IPTG was added and the cultures were left with shaking at 37 °C overnight. Because the C53H mutant enzyme formed inclusion bodies when overexpressed at 37 °C, SØ5201/pTrcC53H was grown and induced overnight at 20 °C. Otherwise it was treated as described below. Cells were harvested by centrifugation, washed once with 0.9% NaCl, resuspended in 3−4 volumes 50 mM Tris-HCl, pH 7.6, and disrupted by sonic oscillations at 4 °C. Cellular debris was removed by centrifugation, and streptomycin sulfate was added to a final concentration of 1%. Following centrifugation, the wild-type T-CDA was purified as described previously (*26*). The R56A and R56Q mutant enzymes were purified by two subsequent fast protein liquid chromatographic steps. First, they were eluted from a Q5 (BioRad) ion-exchange column with a linear gradient of NaCl (0−0.4 M) in 20 mM Tris-HCl, pH 7.6. Following dialysis against 20 mM Tris-HCl, pH 7.2, the fractions containing the enzyme were applied to a Q6 (BioRad) ion-exchange column in the same buffer and the enzyme was eluted with the same linear NaCl gradient as before. Fractions containing the enzyme were pooled, concentrated by pressure filtration, and applied to G-75 Sephadex (Pharmacia) column (2.5 × 90 cm) equilibrated and eluted with 50 mM Tris-HCl, pH 7.6. The enzyme fractions were made 2 mM in DTT and concentrated by pressure filtration to 1−3 mg of protein per milliliter. The streptomycin sulfate supernatants of R56D, C53H, and C53H/R56Q were first applied to a DEAE-cellulose (DE52) column (1.5 × 15 cm) and eluted with a linear gradient of NaCl (0−0.35 M) in 50 mM Tris-HCl, pH 7.6. Fractions containing the mutant protein were pooled, concentrated, and gel-filtrated on the G-75 Sephadex column as described above. Subsequently, the mutant enzymes were further purified on a Q5 ion-exchange column by elution with a 0−0.4 M NaCl gradient in 20 mM Tris-HCl, pH7.6.

Enzyme Assays. The deamination of cytidine and deoxycytidine in 0.1 M Tris-HCl buffer pH 7.6 and pH 7.8, respectively, was monitored by the absorbance at 290 nm

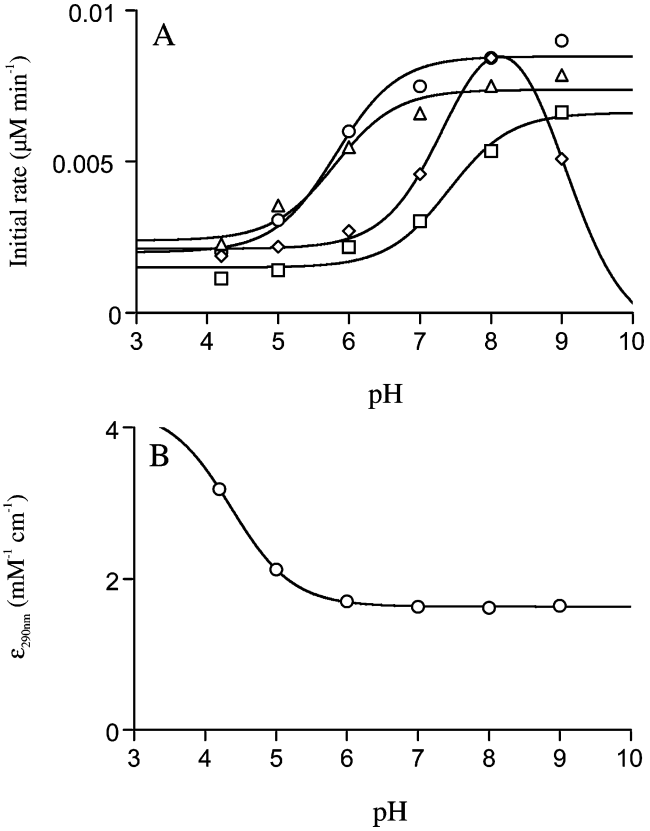

FIGURE 3: (A) Initial velocities for wild-type *B. subtilis* T-CDA (circles), R56A (squares), R56Q (triangles), and C53H/R56Q (diamonds) as a function of pH. Assays were carried out at 25 °C as described in Materials and Methods and initiated by the addition enzyme, except for the C53H/R56Q enzyme, in which assays were initiated by the addition of substrate to a mixture of buffer and enzyme preincubated at 25 °C for 5 min. The following protein concentrations were used to give comparable initial velocities: 0.26 μg/mL (wild-type), 10 μg/mL (R56A), 5.2 μg/mL (R56Q), and 0.20 mg/mL (C53H/R56Q). A fit to the data points yielded the following apparent pK_a values: 5.8 ± 0.2, 7.4 ± 0.2, 6.0 ± 0.2 for wild-type *B. subtilis* T-CDA, R56A, and R56Q, respectively. The C53H/R56Q line is interpolated to fit the measured points. (B) $\Delta\epsilon_{290}$ for the deamination of deoxycytidine as a function of pH determined as described in Materials and Methods.

($\Delta\epsilon_{\text{cytidine}} = 1.79\ M^{-1}\ cm^{-1}$, $\Delta\epsilon_{\text{deoxycytidine}} = 1.69\ M^{-1}\ cm^{-1}$) using cuvettes maintained at 25 °C. Data from initial velocity determinations were fitted with the BIOSOFT program UltraFit 3.0 for Macintosh to the Michaelis−Menten equation: $v_0 = V_{max}S(K_M + S)^{-1}$. The influence of pH on the enzymatic activity was determined in solutions buffered by potassium phosphate (0.02 M) in the pH range between 4.2 and 9. The reaction was monitored at 290 nm, by the disappearance of deoxycytidine (1.9×10^{-5} M), using cuvettes maintained at 25 °C. Reaction rates were calculated from the $\Delta\epsilon_{290}$ values determined in the 4.2−9 pH range in 0.02 M potassium phosphate buffer as shown in Figure 3 b. The apparent pK_a values were obtained from calculations with UltraFit 3.0.

Gel Filtration. The molecular mass of recombinant T-CDA was determined by gel filtration using Superose 12 HR 10/30 (Pharmacia) connected to a fast protein liquid chromatography system (Bio-Rad, CA) at room temperature. The column was equilibrated and eluted with 50 mM Tris-HCl, pH 7.8. The following marker proteins were used: carbonic anhydrase (29 kDa), RNaseA (13.7 kDa), and bovine serum albumin (66 kDa). The purity of the enzymes and the subunit molecular masses were determined by SDS−PAGE as described by Laemmli (*27*) using 15% acrylamide. The markers were Bio-Rad low range. Proteins were visualized by Coomassie blue.

Zinc Analysis. A thin film of 30−60 μg of R56A, R56Q, R56D, and C53H/R56Q that had been dialyzed against 10 mM Tris-nitrate buffer pH 7.0 (metal free) was used in an energy-dispersive X-ray fluorescence spectroscopy analysis. The analysis was performed by Jens Laursen, Department of Mathematics and Physics, The Royal Veterinary and Agricultural University, Copenhagen, Denmark. The sulfur signal of the protein was used as reference for the zinc content.

Crystallization. Crystals of the recombinant mutant enzymes, R56A and R56Q, were obtained as described for the wild-type *B. subtilis* T-CDA (*2*). The crystals used for data collection were grown by vapor diffusion in drops formed by mixing 2 μL of 4.6 mg/mL CDA and 5 mM THU in 50 mM Tris-HCl, pH 7.6 with 2 μL of mother liquor. The mother liquor was composed of 10 mM calcium chloride, 0.1 M sodium acetate, pH 4.6, and 17 or 23% MPD (R56A and R56Q, respectively). The hanging drops were equilibrated over 1 mL of mother liquor at room temperature.

C53H/R56Q could not be crystallized under the same conditions. Hence, a vapor diffusion screening procedure with Crystal screen I from Hampton Research (*28*) was performed using the same protein and THU concentrations as for the two other mutant enzymes. Crystals suitable for diffraction studies were obtained at room temperature with solution 23 (0.2 M magnesium chloride, 0.1 M HEPES, pH 7.5, 30% v/v poly(ethylene glycol) 400). These crystals grew to a size of $0.5 \times 0.25 \times 0.1$ mm in 3 days.

Data Collection. Diffraction data for R56A and R56Q were collected on crystals cryocooled to 100 K at beamline I711, MAX-lab, Lund University, Sweden (*29*) using a CCD detector from MAR Research. C53H/R56Q diffraction data were collected on a crystal cryocooled to 120 K on a MAR345 image plate detector mounted on a copper rotating anode generator from Rigaku (RU300) operating at 46kV/70mA. Auto-indexing, data reduction, and scaling were performed with programs from the HKL-suite (*30*). Statistics on the diffraction data are shown in Table 1. The crystals of the R56A and R56Q mutant enzymes belong to space group *C*2, and they are, like the crystals of wild-type *B. subtilis* CDA, nonmerohedrally twinned (*2*). The data set used in the calculation of *R*-free was the same as used for the wild-type structure; DATAMAN (*31*) was used for the transfer to the mutant data sets. The crystals of C53H/R56Q belong to space group $P3_221$ and diffract well beyond 2.36 Å resolution. However, the long *c*-axis (221.6 Å) prevented data collection to higher resolution.

Structure Determination and Refinement. R56A and R56Q crystallize in the same crystal form as wild-type *B. subtilis* T-CDA with two subunits in the asymmetric unit. Hence, the wild-type *B. subtilis* T-CDA crystal structure (Protein Data Bank accession code 1JTK) could be used directly as model. All water molecules and THU were removed from the wild-type model, and residue Arg56 was replaced by a glycine residue and an alanine residue for R56A and R56Q, respectively. A rigid body refinement, allowing the two

Table 1: Diffraction Data and Refinement Statistics[a]

	R56A	R56Q	C53H/R56Q
Diffraction Data Statistics			
wavelength (Å)	0.968	0.968	1.542
resolution (Å)	20−1.99 (2.04−1.99)	20−1.99 (2.04−1.99)	25−2.36 (2.41−2.36)
space group	*C*2	*C*2	$P3_221$
cell dimensions	$a = 74.7$, $b = 66.4$, $c = 55.4$	$a = 74.9$, $b = 66.1$, $c = 55.5$	$a = b = 62.5$, $c = 221.6$
a, *b*, *c* (Å), α, β, γ (deg)	$\beta = 115.6$	$\beta = 115.6$	$\alpha = \beta = 90$, $\gamma = 120$
Z	8	8	24
R_{linear} (%)[b]	11.4 (38.8)	10.6 (35.1)	5.9 (21.7)
$I/\sigma(I)$	10.8 (1.3)	16.9 (3.2)	29.8 (6.9)
completeness (%)	94.0 (54.0)	100 (99.4)	98.9 (83.9)
no. of reflections	67496	107726	146498
no. of unique reflections	15794	16761	21401
Refinement Statistics			
no. of reflections	15662	16757	21345
working set	14915	15980	20274
test set	747	777	1071
resolution (Å)	19.96−1.99 (2.11−1.99)	19.95−1.99 (2.11−1.99)	24.66−2.36 (2.51−2.36)
no. of atoms	2126	2131	4114
R-factor (%)[c]	18.8 (26.7)	19.1 (19.2)	21.3 (24.1)
R-free (%)[d]	21.1 (27.3)	20.7 (20.2)	24.5 (27.6)
average B-factor (Å^2)	23.7	23.6	31.5
average B-factor protein (Å^2)	23.0	22.9	31.6
average B-factor water (Å^2)	33.8	33.3	32.6
average B-factor THU and zinc (Å^2)	22.3	22.4	27.5
bond length rmsd from ideal (Å)	0.006	0.004	0.006
bond angle rmsd from ideal (deg)	1.2	1.1	1.2

[a] Values in parentheses are data for the highest resolution shell. [b] $R_{linear} = \sum|I - \langle I\rangle|/\sum I$, where the sums are over all reflections of intensity *I*. [c] *R*-factor $= \sum_{work}||F_{obs}| - k|F_{calc}||/\sum_{work}F_{obs}$. [d] *R*-free $= \sum_{test}||F_{obs}| - k|F_{calc}||/\sum_{test}F_{obs}$, where F_{obs} and F_{calc} are observed and calculated structure factors, respectively, *k* is the scale factor, and the sums are over all reflections in the working set and test set, respectively.

protein chains in the asymmetric unit to move separately, was performed with CNS (*32*).

The structure of C53H/R56Q, which crystallizes in a different space group from the other two mutant enzymes, was determined by the molecular replacement method using the program EPMR (*33*). The wild-type *B. subtilis* T-CDA model contains half a tetramer, and this was used as a search model with residues 53 and 56 substituted by alanine residues. The correct molecular replacement solution contained two copies of the search model, i.e., a full tetramer in the asymmetric unit (correlation coefficient 54.3%, *R*-value 40.7%). For all three structures, the difference electron density map showed clear electron density for the side chains of the mutated residues and THU. The correct side chains and THU were introduced and minor rebuilding was done, all with the program O (*34*). Further positional refinement, B-value refinement, and water-picking with restrained noncrystallographic symmetry (NCS) were performed with CNS (*32*). For R56A and R56Q water molecules related by NCS were identified with the program WATNCS (*35*) and added to the NCS restraints list. As refinement progressed, the NCS restraints were relaxed. The quality of the models was controlled with PROCHECK (*36*), and the final models have all their residues within the allowed regions in the Ramachandran plot. The structures of R56A and R56Q contain two subunits of the tetramer in the asymmetric unit. Both R56A and R56Q models contain 260 amino acid residues, whereas the six C-terminal residues are not visible in the electron density map, analogous to the wild-type structure. Furthermore, these two models hold two zinc ions, and two THU molecules, 148 water molecules for R56A, and 145 water molecules for R56Q, respectively. The C53H/R56Q structure contains four subunits, i.e., a full tetramer, with in total 522 amino acid residues. This model also contains four zinc ions, four THU molecules, one Tris molecule, and 98 water molecules. Refinement statistics are shown in Table 1.

RESULTS AND DISCUSSION

Rationale. One of the distinct characteristics of T-CDA as compared to D-CDA is that the catalytic zinc ion in T-CDA is liganded to three cysteine residues, whereas in D-CDA the zinc ligands are one histidine and two cysteine residues. Thus, T-CDA is faced with an extra negative charge in the active site, which would be expected to decrease the ability of the zinc ion to activate the attacking water molecule. To investigate the importance of the conserved Arg56 residue and the dipole moments from two α-helices in neutralizing the extra negative charge in T-CDA, a number of mutants with substitutions of the Arg56 residue were constructed. Furthermore, the ability of a D-CDA zinc ligand combination (one histidine and two cysteine residues) to function in a T-CDA was investigated in mutant enzymes containing a Cys53-to-His substitution.

Protein Expression and Purification. The pyrimidine requiring host strains of *E. coli*, JF611 and SØ5201, cannot grow with deoxycytidine as the sole pyrimidine source due to a lack of CDA activity. However, the pTrc99-A plasmids harboring either wild-type T-CDA or the R56A, R56Q, and C53H/R56Q mutant T-CDAs grew well with deoxycytidine as the pyrimidine source in the absence of IPTG, indicating that even uninduced expression of CDA from the plasmids was adequate for complementation of the *cdd* mutations of the host strains. In contrast, strains expressing the C53H or R56D mutant enzymes did not grow on deoxycytidine, either with or without induction by IPTG.

Both wild-type and mutant enzymes were purified as described in Materials and Methods. As judged from SDS−

Table 2: Steady State Kinetics of Various *B. subtilis* T-CDAs with Cytidine and Deoxycytidine as the Variable Substrate

	cytidine		deoxycytidine	
	K_m (μM)	V_{max}[a]	K_m (μM)	V_{max}[a]
Wild-type	216 ± 58	184 ± 18	236 ± 140	230 ± 50
R56A	140 ± 29	7.5 ± 0.5	160 ± 70	8.0 ± 1.3
R56Q	267 ± 100	29 ± 4	230 ± 160	19 ± 5
R56D		nd[b]		nd[b]

[a] μmol of deaminated substrate min^{-1} (mg of protein)$^{-1}$. [b] nd, not detectable, the specific activity was less than 0.01 μmol min^{-1} (mg of protein)$^{-1}$.

PAGE of the final preparations, the wild-type T-CDA, R56Q, and R56A were >95% pure, C53H/R56Q was about 90% pure, and C53H and R56D were about 80% pure (data not shown). The purifications were followed by SDS−PAGE and, when possible, also by enzyme activity measurements. However, no CDA activity was detected with the C53H and R56D mutant enzymes, either with the purified preparations or in assays using crude extracts.

Zinc Analysis. The zinc content of the various mutant enzymes was determined using energy-dispersive X-ray fluorescence spectroscopy. The molar amount of bound zinc per subunit in R56A, R56Q, and C53H/R56Q was found to be 0.9, 1.1, and 1.3, respectively, and hence the same as in the wild-type enzyme within experimental uncertainties (*37*). According to the crystal structure of *B. subtilis* T-CDA, none of these mutations were expected to change the binding of zinc. However, with an extra negative charge introduced near the active site, as in R56D, the energy-dispersive X-ray fluorescence spectroscopy analysis showed 0.2 mol of zinc per subunit. This reduction in the zinc binding capacity of R56D indicates a destabilization of the zinc ion binding site and explains the lack of CDA activity of this mutant enzyme.

Kinetic Properties. The effect of the various mutations on the steady-state saturation kinetics of CDA was investigated using both cytidine and deoxycytidine as the variable substrate (Table 2). With either substrate, the K_m values of R56A and R56Q were not significantly altered compared to the wild-type enzyme, whereas a reduction in the V_{max} values was clearly observed, with V_{max} of R56A being more affected than that of R56Q. Thus, the substrate binding was not affected significantly by the amino acid replacements, whereas the catalytic efficiency was impaired. This is in agreement with the proposed role of Arg56 neutralizing the excess of negative charge (*2*). The dipoles of two α-helices are able to exercise their charge neutralizing role, and this explains why the enzymatic activity may be retained, although diminished. The R56D mutant enzyme in which the positive charge of the arginine residue was substituted with a negative charge, appeared to be inactive, as judged both by lack of enzyme activity of the purified protein, and by the inability of plasmid pTrcR56DCDA to complement the *cdd* mutation of the host strain.

Changing the zinc liganding residue Cys53 to a histidine residue, as is found in D-CDA, resulted in an inactive enzyme, which formed inclusion bodies when overexpressed at 37 °C. However, introduction of a second mutation, changing Arg56 to a glutamine residue, as found in the D-CDA as well, resulted in an enzymatically active form of the protein. The activity of C53H/R56Q was approximately 500-fold lower than the wild-type enzyme, and it did not

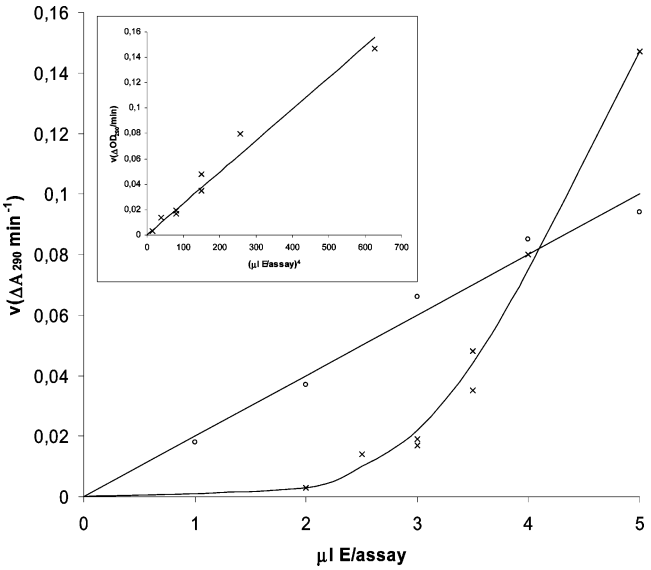

FIGURE 4: *B. subtilis* T-CDA activity as a function of enzyme concentration. Assays were carried out at 25 °C as described in Materials and Methods and initiated by the addition of substrate to a mixture of buffer and enzyme preincubated at 25 °C for 5 min. Initial reaction velocities (v) are given as ΔA_{290}/min. The solutions of purified enzyme were as follows: o−o, wild-type (50 μg of protein/mL); x−x, C53H/R56Q (5.9 mg of protein/mL). The inset illustrates the C53H/R56Q velocities as a function of (μL of enzyme/assay)^4.

display proportionality between activity and enzyme concentration (Figure 4), which precluded any meaningful determination of V_{max} and K_m. As shown in the inset of Figure 4, a replot of the same data indicated that the activity of the mutant enzyme was proportional to [Enz]^4. This may imply, that the equilibrium between an inactive monomeric and an active tetrameric form of T-CDA is significantly displaced toward the inactive monomers for the C53H/R56Q mutant enzyme.

Structures of the Mutant Enzymes. The crystal structures of three of the mutant T-CDAs were determined (R56A, R56Q, and C53H/R56Q). R56A and R56Q crystallized in the same space group (*C*2) as the wild-type enzyme with two subunits in the asymmetric unit, whereas C53H/R56Q could not crystallize in this crystal form but was crystallized in another space group ($P3_221$) with a full tetramer in the asymmetric unit. Compared to the wild-type enzyme, the overall tetrameric structures have rmsd values of 0.20 Å (R56A), 0.39 Å (R56Q), and 0.58 Å (C53H/R56Q) for 520 equivalent Cα-atoms as determined using default parameters in O (*34*). Major differences were found in the active site area as demonstrated in Figure 2, which shows the active sites and the hydrogen bonding networks. The main difference between R56A (Figure 2b) and the wild-type enzyme (Figure 2a) is that the alanine residue, in contrast to Arg56, cannot form hydrogen bonds to the zinc ion liganding cysteine residues Cys53 and Cys89. The glutamine residue Gln56 in R56Q, on the other hand, forms one hydrogen bond to Cys89 (Figure 2c). This explains why R56A displays a lower V_{max} than R56Q. The hydrogen bond between Gln56 and Cys89 in R56Q modulates the reactivity of the zinc ion yielding a more active enzyme relative to R56A, which solely depends on charge neutralization by the dipoles from the two α-helices. The hydrogen bond to Cys89 in R56Q is also present in C53H/R56Q (Figure 2d). A negatively charged

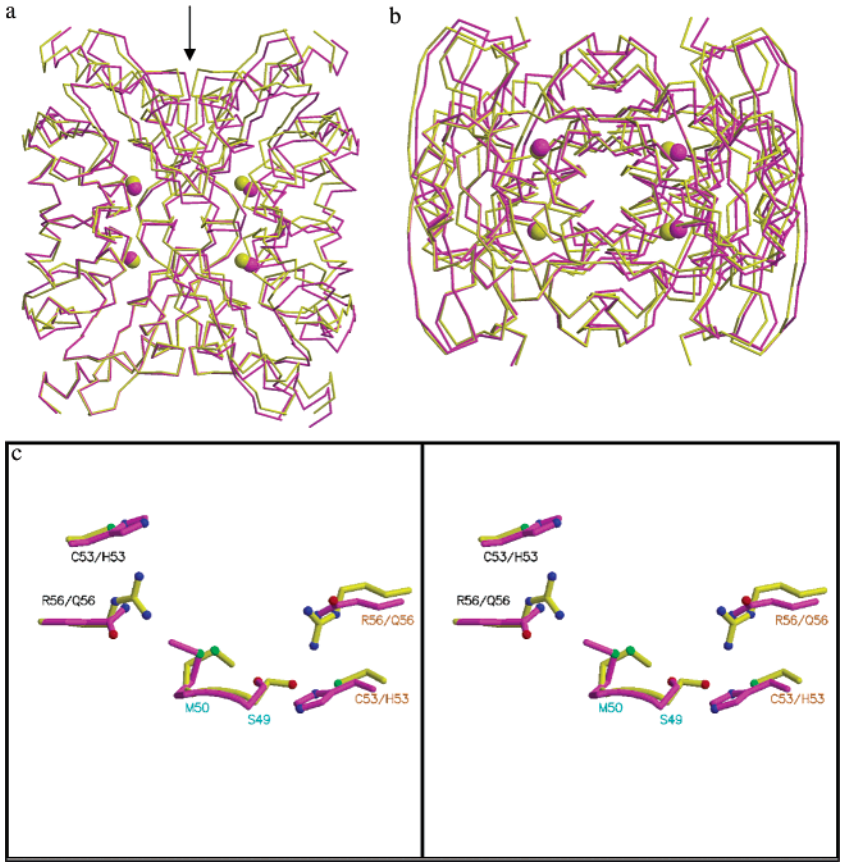

FIGURE 5: Wild-type *B. subtilis* T-CDA (yellow) and C53H/R56Q (magenta) with one of the four subunits superimposed. Panels (a) and (b) show the Cα-trace of the structures in perpendicular views, where (b) is displayed in the direction of the arrow in (a). The zinc ions are displayed as spheres. (c) The vicinity of the mutated residues in stereoview. Residues from three different subunits of the tetramer are shown with text in black, cyan, and orange, respectively. The pictures were prepared with MOLSCRIPT (*38*) and Raster3D (*39*).

aspartate residue at position 56, as in R56D, would on the other hand most likely disrupt the charge distribution in the active site, which leads to an impaired capacity of R56D to bind zinc.

The incompatibility in size of Arg56 and His53 may be one of the reasons to the formation of inclusion bodies and the lack of activity of C53H. A comparison of the wild-type and C53H/R56Q tetramers reveals a small displacement that is visible when one of the four subunits of the tetramer from the two structures are superimposed, as in Figure 5a,b. This displacement may be described as a clockwise rotation of C53H/R56Q relative to the wild-type enzyme as seen in Figure 5a. The rotation destroys the perfect 2-fold symmetry present in the wild-type crystal structure and explains why C53H/R56Q could not be crystallized in the same manner. To give a comparable picture between structures refined to different resolution, the B-values were scaled to the overall B-values in the respective structures. The core of the wild-type T-CDA structure has generally low B-values, which also is the case for R56A and R56Q, but is different in the C53H/R56Q structure. The C53H/R56Q structural core has comparably much higher B-values that indicate higher mobility in this part of the structure. The introduction of a histidine residue at position 53 invokes the movements of residues Ser49 and Met50 illustrated in Figure 5c. If Arg56 is not simultaneously replaced by a shorter residue, such as glutamine, there is no space to accommodate Met50. This may explain the problems encountered when the single mutant enzyme C53H is expressed. The two residues (Ser49 and Met50) also have significantly higher B-values in the C53H/R56Q structure than in the wild-type structure. The high mobility in the structural core supports the apparent dissociation of the C53H/R56Q tetramer at low protein concentration. Zinc ions coordinated to three cysteine residues are most commonly found as structural zinc ions (*4*). The destabilization of the C53H/R56Q tetramer suggests that the zinc ion in T-CDA has both a catalytic and a structural role. A similar role for a catalytic zinc ion liganded to three cysteine residues was also suggested for the Blasticidin S deaminase from *Asperigillus terreus* (*7*). The single point mutation in T-CDA where Cys53 is replaced with a histidine residue may perturb the structure even more, and this disruption could be the cause of formation of inclusion bodies in the expression of C53H.

pH Dependence. The changes introduced in the surroundings of the catalytic zinc ion in the mutant T-CDAs should also change the pK_a value of the coordinated water molecule, e.g., one would expect that a reduction of the positive charge around the zinc ion should lead to a higher pK_a value. The influence of pH value on the enzyme activity has previously been investigated for D-CDA from *E. coli* and T-CDA from *B. subtilis* (*37*). From these measurements, it was possible to deduce the apparent pK_a values 4.7 for D-CDA and 5.4 for T-CDA. The higher pK_a value for T-CDA may be an effect of the difference in zinc coordination caused by the replacement of a histidine with a cysteine. We have conducted a similar investigation of the wild-type and the R56A, R56Q, and C53H/R56Q mutant T-CDAs, and results

are shown in Figure 3. The double mutant enzyme C53H/R56Q has a dramatic drop in activity at pH values above 8, which could be caused by a destabilization of the tetramer as is suggested by its crystal structure. The apparent pK_a value 5.8 for the wild-type enzyme is in accordance with the results from the previous study and only slightly lower than the pK_a value of 6.0 deduced for the R56Q mutant T-CDA, which does not have the charge but is able to maintain a hydrogen bond to the third cysteine residue as revealed by its structure. The apparent pK_a value for the R56A enzyme is reduced by one pH unit relative to the wild-type enzyme which reflects the more negatively charged zinc ion. It is interesting that the positive charge exerted by the helix dipoles more than compensates the additional charge of the third cysteine residue giving an apparent pK_a value around 7 for the coordinated water molecule.

CONCLUSIONS

The T-CDA active site contains additional negative charge compared to D-CDA originating from the change of a zinc liganding histidine residue, characteristic of D-CDA, to a consensus cysteine residue in T-CDA. From the structure of *B. subtilis* T-CDA, the dipoles of two α-helices together with the conserved arginine residue Arg56 were identified as important in neutralizing the additional negative charge (*2*). This proposal has been tested by site-directed mutagenesis of the Arg56 residue of *B. subtilis* T-CDA. The R56A and R56Q mutant enzymes are not affected in binding of the substrate, but they display a decreased catalytic efficiency, which we interpret as originating from the nonexisting or diminished ability of charge neutralizing by Arg56 for R56A and R56Q, respectively. In the case of R56A, that has no hydrogen-binding properties, the remaining catalytic capability is a result of the dipole moment from two α-helices. Furthermore, R56A displays an increased apparent pK_a value compared to wild-type *B. subtilis* T-CDA and R56Q. This supports the nonexisting ability of charge neutralizing from Arg56 for R56A. The addition of an extra negative charge, as in R56D, results in a catalytically inactive enzyme with impaired zinc binding capacity, emphasizing the importance of Arg56 and zinc for the catalytic function. Attempts to express and purify C53H were unsuccessful. However, the double mutant enzyme C53H/R56Q, in which two of the residues in the active site have been replaced by their D-CDA counterparts, is enzymatically active, although with significantly reduced specific activity. C53H/R56Q also displays reduced activity at high pH and an increased apparent pK_a value compared to wild-type T-CDA. The kinetic and structural results support that the mutations have caused an impaired stability of the tetrameric arrangement of C53H/R56Q. This can be explained if the zinc ion coordinated by three cysteine residues in T-CDA also plays a structural role.

ACKNOWLEDGMENT

We thank Lisbeth Stauning for excellent technical assistance and Dr. Leila Lo Leggio for help during data collection. We acknowledge the access to synchrotron radiation at beamline I711, MAX-laboratory, Lund, the support from the EC Access to Research Infrastructure (ARI) program, and the support from the Danish Natural Science Research Council to DANSYNC.

REFERENCES

1. Neuhard, J. (1983) Utilization of preformed pyrimidine bases and nucleosides in *Metabolism of Nucleotides, Nucleosides and Nucleobases in Microorganisms* (Munch-Pedersen, A., Ed.) pp 95−148, Academic Press, London.
2. Johansson, E., Mejlhede, N., Neuhard, J., and Larsen, S. (2002) Crystal structure of the tetrameric cytidine deaminase from *Bacillus subtilis* at 2.0 Å resolution. *Biochemistry 41*, 2563−2670.
3. Betts, L., Xiang, S., Short, S. A., Wolfenden, R., and Carter, C. W., Jr. (1994) Cytidine deaminase. The 2.3 Å crystal structure of an enzyme: transition-state analog complex. *J. Mol. Biol. 235*, 635−656.
4. Vallee, B. L., and Auld, D. S. (1990) Zinc coordination, function, and structure of zinc enzymes and other proteins. *Biochemistry 29*, 5647−5659.
5. Kimura, M., Sekido, S., Isogai, Y., and Yamaguchi, I. (2000) Expression, purification, and characterization of blasticidin S deaminase (BSD) from Aspergillus terreus: the role of catalytic zinc in enzyme structure. *J. Biochem. 127*, 955−963.
6. Nakasako, M., Kimura, M., and Yamaguchi, I. (1999) Crystallization and preliminary X-ray diffraction studies of blasticidin S deaminase from *Aspergillus terreus*. *Acta Crystallogr., Sect. D: Biol. Crystallogr. 55*, 547−548.
7. Mejlhede, N., and Neuhard, J. (2000) The role of zinc in *Bacillus subtilis* cytidine deaminase. *Biochemistry 39*, 7984−7989.
8. Ireton, G. C., McDermott, G., Black, M. E., and Stoddard, B. L. (2002) The structure of *Escherichia coli* cytosine deaminase. *J. Mol. Biol. 315*, 687−697.
9. Ko, T.-P., Lin, J.-J., Hu, C.-H., Hsu, Y.-H., Wang, A., H.-J., and Liaw, S.-H. (2003) Crystal structure of yeast cytosine deaminase. Insights into enzyme mechanism and evolution. *J. Biol. Chem. 278*, 19111−19117.
10. Ireton, G. C., Black, M. E., and Stoddard, B. L. (2003) The 1.14 Å crystal structure of yeast cytosine deaminase: evolution of nucleotide salvage enzymes and implications for genetic chemotherapy. *Structure 11*, 961−972.
11. Moore, J. T., Silversmith, E. E., Maley, G. F., and Maley F. (1993) T4-phage deoxycytidylate deaminase is a metalloprotein containing two zinc atoms per subunit. *J. Biol. Chem. 268*, 2288−2291.
12. Beck, C. F., Eisenhardt, A. R., and Neuhard, J. (1975) Deoxycytidine triphosphate deaminase of *Salmonella typhimurium*. Purification and characterization. *J. Biol. Chem. 250*, 609−616.
13. Li, H., Xu, H., Graham, D. E., and White, R. H. (2003) The *Methanococcus jannaschii* dCTP deaminase is a bifunctional deaminase and diphosphatase. *J. Biol. Chem. 278*, 11100−11106.
14. Björnberg, O., Neuhard, J., and Nyman, P. O. (2003) A bifunctional dCTP deaminase-dUTP nucleotidohydrolase from the hyperthermophilic archaeon *Methanocaldococcus jannaschii*. *J. Biol. Chem. 278*, 20667−20672.
15. Johansson, E., Björnberg, O., Nyman, P. O., and Larsen, S. (2003) Structure of the bifunctional dCTP deaminase-dUTPase from *Methanocaldococcus jannaschii* and its relation to other homotrimeric dUTPases. *J. Biol. Chem. 278*, 27916−27922.
16. Huffman, J. L., Li, H., White, R. H., and Tainer, J. A. (2003) Structural basis for recognition and catalysis by the bifunctional dCTP deaminase and dUTPase from *Methanococcus jannaschii*. *J. Mol. Biol. 331*, 885−896.
17. Christianson, D. W., and Cox, J. D. (1999) Catalysis by metal-activated hydroxide in zinc and manganese metalloenzymes. *Annu. Rev. Biochem. 68*, 33−57.
18. Christianson, D. W., and Fierke, C. A. (1996**)** Carbonic Anhydrase: Evolution of the zinc binding site by nature and by design. *Acc. Chem. Res. 29*, 331−339.
19. Clark, D. J., and Maaløe, O. (1967) DNA replication and the division cycle in *Escherichia coli*. *J. Mol. Biol. 23*, 99−112.
20. Hove-Jensen, B., and Maigaard, M. (1993) *Escherichia coli* rpiA gene encoding ribose phosphate isomerase A. *J. Bacteriol. 175*, 5628−5638.
21. Sambrook, J., Fritsch, E. F., and Maniatis, T. (1989) *Molecular Cloning: A Laboratory Manual*, 2nd ed., Cold Spring Harbor Laboratory, Cold Spring Harbor, NY.
22. Birnboim, H. C., and Doly, J (1979) A rapid alkaline extraction procedure for screening recombinant plasmid DNA. *Nucleic Acids Res. 7*, 1513−1523.
23. Sanger, J., Nicklen, S., and Coulson, A. R. (1977) DNA sequencing with chain-terminating inhibitors. *Proc. Natl. Acad. Sci. U.S.A. 74*, 5463−5467.

24. Song, B. H., and Neuhard, J. (1989) Chromosomal location, cloning and nucleotide sequence of the *Bacillus subtilis* cdd gene encoding cytidine/deoxycytidine deaminase. *Mol. Gen. Genet. 216*, 462−468.
25. Vincenzetti S., Cambi, A., Maury, G., Bertorelle, F., Gaubert, G., Neuhard, J., Natalinin, P., Salvatori, D., Sanctis, G., and Vita, A. (2000) Possible role of two phenylalanine residues in the active site of human cytidine deaminase. *Protein Eng. 13*, 791−799.
26. Mejlhede, N., Atkins, J. F., and Neuhard, J. (1999) Ribosomal −1 frameshifting during decoding of *Bacillus subtilis* cdd occurs at the sequence CGA AAG. *J. Bacteriol. 181*, 2930−2937.
27. Laemmli, U.K. (1970) Cleavage of structural proteins during the assembly of the head of bacteriophage T4. *Nature 277*, 680−685.
28. Jancarik, J., and Kim, S. H. (1991) Sparse matrix sampling: a screening method for crystallization of proteins. *J. Appl. Crystallogr. 24*, 409−411.
29. Cerenius, Y., Ståhl, K., Svensson, L. A., Ursby, T., Oskarsson, Å., Albertsson, J., and Liljas, A. (2000) The crystallography beamline I711 at MAX II. *J. Synchrotron Radiat. 7*, 203−208.
30. Otwinowski, Z., and Minor, W. (1997) Processing of X-ray diffraction data collected in oscillation mode. *Methods Enzymol. 276*, 307−326.
31. Kleywegt, G. J., and Jones, T. A. (1996) xdlMAPMAN and xdlDATAMAN − Programs for reformatting, analysis and manipulation of biomacromolecular electron-density maps and reflection data sets. *Acta Crystallogr., Sect. D: Biol. Crystallogr. 52*, 826−828.
32. Brünger, A. T., Adams, P. D., Clore, G. M., DeLano, W. L., Gros, P., Grosse-Kunstleve, R. W., Jiang, J.-S., Kuszewski, J., Nilges, M., Pann, N. S., Read, R. J., Rice, L. M., Simonson, T., and Warren, G. L. (1998) Crystallography & NMR System: A new software suite for macromolecular structure determination. *Acta Crystallogr., Sect. D: Biol. Crystallogr. 54*, 905−921.
33. Kissinger, C. R., Gehlhaar, D. K., and Fogel, D. B. (1999) Rapid automated molecular replacement by evolutionary search. *Acta Crystallogr., Sect. D: Biol. Crystallogr. 55*, 484−491.
34. Jones, T. A., Zou, J., Cowan, S., and Kjeldgaard, M. (1991) Improved methods for building protein models in electron density maps and the location of errors in these models. *Acta Crystallogr., Sect. A: Found. Crystallogr. 47*, 110−119.
35. Collaborative Computational Project, No. 4 (1994) The CCP4 suite: programs for protein crystallography. *Acta Crystallogr., Sect. D: Biol. Crystallogr. 50*, 760−763.
36. Laskowski, R. A., MacArthur, M. W., Moss, D. S., and Thornton, J. M. (1993) PROCHECK: a program to check the stereochemical quality of protein structures. *J. Appl. Crystallogr. 26*, 283−291.
37. Carlow, D. C., Carter, C. W., Jr., Mejlhede, N., Neuhard, J., and Wolfenden, R. (1999) Cytidine deaminases from B. subtilis and E. coli: compensating effects of changing zinc coordination and quaternary structure. *Biochemistry 38*, 12258−12265.
38. Kraulis, P. J. (1991) MOLSCRIPT: a program to produce both detailed and schematic plots of protein structures. *J. Appl. Crystallogr. 24*, 946−950.
39. Merrit, E. A., and Bacon, D. J. (1997) Raster3D: Photorealistic molecular graphics. *Methods Enzymol. 277*, 505−524.

BI035893X